Article

Modulation instability of hydro-elastic waves blown by a wind with a uniform vertical profile

S. Boral [1]*, T. Sahoo [1] and Y. Stepanyants [2,3]

[1] Department of Ocean Engineering and Naval Architecture, Indian Institute of Technology Kharagpur, Kharagpur 721302, India; susamboral@gmail.com (S. Boral); tsahoo1967@gmail.com(T. Sahoo)
[2] School of Sciences, University of Southern Queensland, Toowoomba, West St., QLD, 4350, Australia
[3] Department of Applied Mathematics, Nizhny Novgorod State Technical University n.a. R.E. Alekseev, Nizhny Novgorod, Russia; Yury.Stepanyants@usq.edu.au

* Correspondence: susamboral@gmail.com

Abstract: An interesting physical phenomenon was recently observed when a fresh-water basin is covered by a thin ice film that has properties similar to that of a rubber membrane. Surface waves can be generated under the action of wind on the air-water interface that contains an ice film. The modulation property of hydro-elastic waves (HEWs) in deep water covered by thin ice film blown by the wind with a uniform vertical profile is studied here in terms of the air-flow velocity versus a wavenumber. The modulation instability of HEWs is studied through the analysis of coefficients of the nonlinear Schrödinger (NLS) equation with the help of the Lighthill criterion. The NLS equation is derived using the multiple scale method in the presence of airflow. It is demonstrated that the potentially unstable hydro-elastic waves with negative energy appear for relatively small wind speeds, whereas the Kelvin–Helmholtz instability arises when the wind speed becomes fairly strong. Estimates of parameters of modulated waves for the typical conditions are given.

Keywords: Wind wave, Ice cover, Vortex sheet, Negative energy wave, Modulation instability

1. Introduction

For certain weather conditions, an interesting phenomenon can be observed when a water basin is covered by a thin ice film having elastic properties similar to that of polymer in which the thickness of the ice film varies from 1 to 5 mm – see, for example, the movie https://news.mail.ru/society/40290629/. Due to the unusual behaviour of such an ice cover which resembles a rubber membrane, it is referred to as "rubber ice". Under the influence of external forces, a wave motion can arise on the water surface covered by an ice film. Wave perturbations, in this case, are very similar to flexural-gravity waves (FGWs) in the oceans covered by floating ice-sheets [1–4] except some specifics caused by much less ice-film elasticity in comparison with the ice-plate rigidity and are referred to as hydro-elastic waves (HEWs). The softer properties of ice rubber in comparison with oceanic ice results in the possibility to excite HEWs on a water surface even by the relatively moderate

Definitions/logo-updates.pdf

Citation: Boral, S.; Sahoo, T.; Stepanyants, Y. Title. *Preprints* , *0*, 0.

Received:
Accepted:
Published:

Publisher's Note: MDPI stays neutral with regard to jurisdictional claims in published maps and institutional affiliations.

Preprints (www.preprints.org) | NOT PEER-REVIEWED | Posted: 2 November 2021 doi:10.20944/preprints202111.0042.v1

wind similar to the generation of gravity-capillary waves. Wind-generated waves can be a subject of modulation instability in the result of which high-amplitude solitary waves can arise. This makes topical the study of conditions of modulation instability. In the case of surface waves without an ice cover the comprehensive study of modulation instability of gravity-capillary waves was undertaken by several authors [5–7]. In the recent paper [8], this study was extended to include the influence of wind in the simplest model of uniform airflow with the tangential discontinuity at the air-water interface. Weakly non-linear modulated waves in the ice-covered ocean were studied by Guyenne & Părău [9] within the framework of the nonlinear Schrödinger (NLS) equation. In the paper by Il'ichev [10], modulated solitary waves of an arbitrary amplitude in the form of "bright" solitons were obtained by taking into account the effects of the ice compression and ice-plate inertia. In the recent publication [11], Il'ichev considered strongly nonlinear envelop solitary wave for the particular carrier wavelength that corresponds to the minimum of the phase speed within the framework of the primitive Euler equation. Then, a similar solution in the form of NLS soliton was derived within the weakly nonlinear theory in the long-wave approximation and it was shown that both solutions are close to each other for moderate depths of water basins. The general analysis of modulation instability of oceanic waves with ice compression and ice-plate inertia in the water of finite depth was carried out recently in [12].

The influence of the wind on oceanic waves covered by a thick ice plate is, apparently, negligible but it is not the case when surface waves are considered in basins covered by a thin film of rubber ice. Such situations can be of particular importance for fresh-water basins such as lakes, rivers, artificial reservoirs, etc. Therefore, it is worth studying the modulation instability of HEWs in water basins covered by a film of rubber ice.

A wind profile over a flexible surface is usually non-uniform which makes it difficult to study waves in shear flows. However, it is feasible to construct a simpler wind model with a uniform vertical profile to evaluate the basic effects generated by airflow over

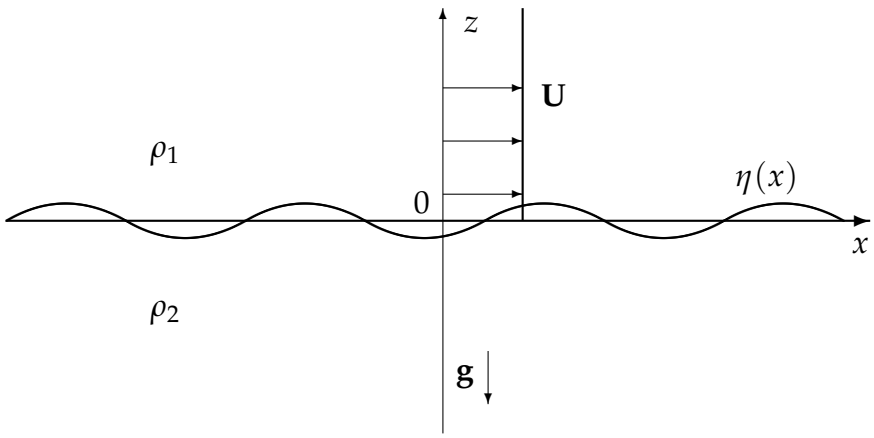

Figure 1. Schematic of the air flow above the ice covered deep water

Preprints (www.preprints.org) | NOT PEER-REVIEWED | Posted: 2 November 2021 doi:10.20944/preprints202111.0042.v1

the water surface as shown in Fig. 1. In hydrodynamics, a shear flow with tangential discontinuity of velocity plays an important role as the reference model which allows one to investigate the basic physical phenomena of wave-current interaction and acquire an insight into such a complex field (see, for example, [13,14]). This model is fascinating because of its simplicity as well as its far-reaching effects on the understanding of wave energy propagation. In particular, it can provide simple explanations about negative energy waves [15], wave-induced currents [16] and over reflection [17,18]. Besides, when the wavelength of interfacial disturbances is considerably larger than the characteristic width of the shear flow profile, the tangential discontinuity of the velocity model can be sufficient for the description of physical phenomena within certain limits of spatial and temporal settings. The aforementioned model is well studied based on the linear approximation as in [14], whilst the modulation instability of weakly nonlinear wavetrains in the absence of ice film was studied recently by [8]. It is of interest to find the criteria for the occurrence of modulation instability on a water surface in the presence of a thin film of rubber ice. In such cases, one can expect the generation of quasi-stationary nonlinear wavetrains along with envelope solitons which can have large amplitudes. An ensemble of these solitons with random parameters can play a prominent role in the development of severe wave turbulence, at least at low wind speeds [19].

The objective of this manuscript is to investigate the existence of modulation instability on the air-water interface in the presence of rubber ice and provide a comprehensive analysis of the conditions when the tangential discontinuity of velocity increases up to the onset of the Kelvin–Helmholtz-type instability. The subsequent sections of the manuscript are organised as follows: In §2, the physical problem is formulated and the dispersion relation for surface waves in water covered by rubber ice under the influence of wind speed is analysed. The NLS equation for the HEWs in the infinitely deep basin is derived in §3. In §4, the criteria for modulation instability of HEWs are determined. Finally, the results are summarized in the conclusion.

2. The problem formulation

We consider a uniform airflow over infinitely deep water covered by an infinitely extended thin ice plate in a horizontal plane. The air and water are both considered to be incompressible and inviscid with the flow being irrotational. The mathematical model is considered in a two-dimensional Cartesian coordinate frame with the x-axis being directed along the air-water interface covered by thin elastic ice film and the z-axis being directed vertically upward as shown in Fig. 1. Moreover, it is assumed that ρ_1 as the density of the air, ρ_2 as the density of water, ρ_i as the density of ice film with d being the thickness and U being the air/wind speed.

Preprints (www.preprints.org) | NOT PEER-REVIEWED | Posted: 2 November 2021 doi:10.20944/preprints202111.0042.v1

Due to the assumptions that both the air and water are inviscid and their motion as irrotational, the velocity potentials Φ_j in each layer is introduced so that $\mathbf{u}_j = \nabla\Phi_j$, where $j = 1, 2$ with index 1 is associated with the quantities in air, and index 2 is associated with the quantities in water. The governing equations in each layer satisfies the Laplace equation as given by

$$\nabla^2\Phi_j = 0 \quad \text{for} \quad j = 1, 2. \tag{1}$$

Further, it is assumed that the wave perturbation in the vertical direction far away from the interface is negaligible, which yields

$$|\nabla\Phi_1| \to 0 \quad \text{as} \quad z \to \infty, \tag{2}$$

$$|\nabla\Phi_2| \to 0 \quad \text{as} \quad z \to -\infty. \tag{3}$$

The kinematic boundary conditions at the interface yield

$$\left(\frac{\partial}{\partial t} + U\frac{\partial}{\partial x}\right)\eta + \frac{\partial\eta}{\partial x}\frac{\partial\Phi_1}{\partial x} = \frac{\partial\Phi_1}{\partial z} \quad \text{on} \quad z = \eta, \tag{4}$$

and

$$\frac{\partial\eta}{\partial t} + \frac{\partial\eta}{\partial x}\frac{\partial\Phi_2}{\partial x} = \frac{\partial\Phi_2}{\partial z} \quad \text{on} \quad z = \eta, \tag{5}$$

with $\eta(x, t)$ being the ice plate deflection from the horizontal mean position. Moreover, the dynamic boundary condition on the interface $z = \eta$ is given by

$$\begin{aligned}\rho_1\left(\frac{\partial}{\partial t} + U\frac{\partial}{\partial x}\right)\Phi_1 - \rho_2\frac{\partial\Phi_2}{\partial t} + (\rho_1 - \rho_2)g\eta \\ + \frac{1}{2}\{\rho_1|\nabla\Phi_1|^2 - \rho_2|\nabla\Phi_2|^2\} - D\frac{\partial^4\eta}{\partial x^4} - \rho_i d\frac{\partial^2\eta}{\partial t^2} = 0,\end{aligned} \tag{6}$$

where $D = Ed^3/12(1 - \nu^2)$ is the ice-plate rigidity with E being the Young modulus and ν being the Poisson ratio. These quantities are not well determined for the rubber ice. Thus, we can speculate that they are close to the known parameters for the Indian rubber of thickness $d = 1$ mm, $E = 10^7$ Pa, $\nu = 0.47$, and $\rho_i = 917$ kg/m^3. These parametric values are used in the subsequent analysis unless otherwise mentioned.

Considering small-amplitude structural response and linearised theory of water waves, the response of the ice sheet is assumed to be of the form

$$\eta(x, t) = Ae^{\mathrm{i}(kx - \omega t)} + c.c., \tag{7}$$

where $c.c.$ indicates the complex conjugate quantity. The velocity potentials Φ_1 and Φ_2 satisfying the boundary conditions given in Eqs. (4) and (5) along with the far-field

Preprints (www.preprints.org) | NOT PEER-REVIEWED | Posted: 2 November 2021 doi:10.20944/preprints202111.0042.v1

boundary conditions for $z \to \pm\infty$ are related with the ice-sheet deflection η by the relations as given by

$$\Phi_1(x,z,t) = -\frac{\eta + U\eta_x}{k}\, e^{-kz}, \qquad \Phi_2(x,z,t) = \frac{\eta}{k}\, e^{kz}. \tag{8}$$

Substituting Eq. (8) into the dynamic boundary condition as in Eq.(6), the dispersion relation is obtained as

$$G_1(\omega,k) \equiv \frac{\rho_1}{k}(\omega - kU)^2 + \Big(\frac{\rho_2}{k} + \rho_i d\Big)\omega^2 + (\rho_1 - \rho_2)g - Dk^4 = 0. \tag{9}$$

In particular, for $\rho_1 = 0$ in Eq. (9), yields the dispersion relation associated with the flexural gravity waves as given by

$$\omega^2 = \frac{Dk^5 + \rho_2\, gk}{\rho_2 + \rho_i\, d\, k},$$

which is generated due to the interaction of surface gravity waves with a thin floating ice-sheet as in [2–4]. The explicit form of the derivations of wave frequencies $\omega_{1,2}$ in terms of the wavenumber k are obtained by solving Eq. (9) with regard to ω (cf. [14]) and is given by

$$\omega_{1,2} = \frac{akU \pm \sqrt{(1 + a + r\, d\, k/\rho_2)[(1-a)gk + Dk^5/\rho_2] - (1 + r\, d\, k/\rho_2)ak^2U^2}}{1 + a + r\, d\, k/\rho_2}, \tag{10}$$

where $a = \rho_1/\rho_2$ is the stratification ratio, $r = \rho_i/\rho_2$ and $+$ and $-$ sign correspond to ω_1 and ω_2 respectively. The dispersion curves are exhibited in Fig. 2 for different values of wind velocity U. For simplicity, the wavenumber k is assumed to be positive, whilst the frequency ω might be positive or negative. It may be noted that the wave frequency ω is a positive quantity from a physical standpoint, however, the wavenumber $k \in (-\infty, \infty)$ might have either sign.

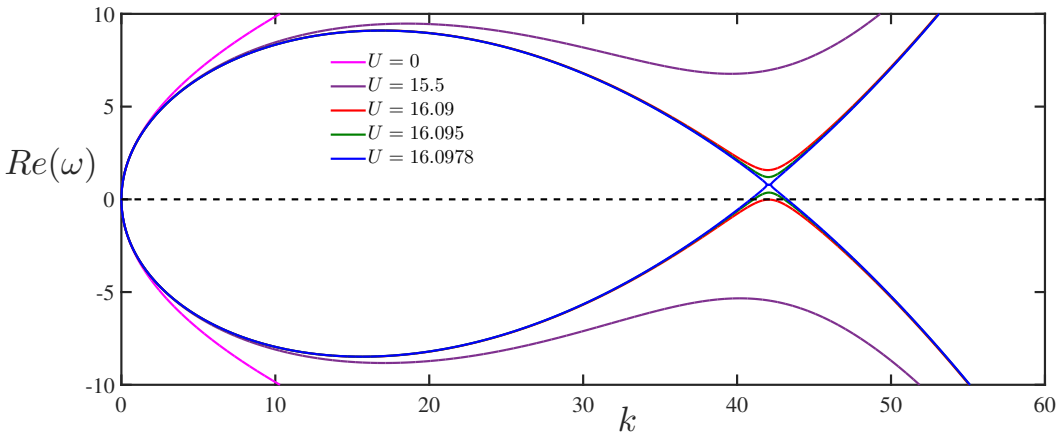

Figure 2. Graphics of the dispersion relations $\omega_1(k)$ (upper branches) and $\omega_2(k)$ (lower branches) for the ice parameters presented above – see after Eq. (6); the values of U are shown in m/s.

Preprints (www.preprints.org) | NOT PEER-REVIEWED | Posted: 2 November 2021 doi:10.20944/preprints202111.0042.v1

As a special case for $U = 0$, Eq. (10) describes two symmetric branches of the dispersion curve with respect to the k-axis, which correspond to the flexural-gravity waves propagating in opposite directions with phase speeds of $V_{ph} = \omega_{1,2}/k$ (see Fig. 2).

On the other hand, the dispersion curves become non-symmetric for $U \neq 0$ due to the wave drift induced by flow. Further, the lower branch of the dispersion curves changes it sign and become positive in the interval $k_1' < k < k_2'$ for $U > U_{c1}(= 16.09)$ m/s. This is illustrated in Fig. 3 for $U = 16.095$ m/s, which represents the magnified portion of Fig. 2.

Besides, the values of k_1' and k_2' can be obtained from Eq. (10) which are real roots of the fourth-degree polynomial in k as given by

$$\frac{D}{\rho_2}k^4 - aU^2k + (1-a)g = 0. \tag{11}$$

Equation (11) can be rewritten in the non-dimensional form

$$p(\kappa) \equiv \kappa^4 - V^2\kappa + 1 = 0, \tag{12}$$

with $\kappa = k\{D/[(1-a)g\rho_2]\}^{1/4}$ and $V^2 = (U^2a\rho_2/D)[(1-a)g\rho_2/D]^{-3/4}$. Figure 4 reveals that the function $p(\kappa)$ has no real root for $V < 1.7547$, whilst it has two distinct positive real roots for $V > 1.7547$.

The critical wind speed U_{c1} is obtained from Eq. (10), where both phase and group velocities vanish and are given by

$$U_{c1} = \left[\frac{4}{3}\frac{1-a}{a}g\left(\frac{4D}{a\rho_2}\right)^{1/3}\right]^{3/8}. \tag{13}$$

It is pertinent to mention that fragment of the dispersion curves for which the frequency changes its sign corresponds to the negative energy waves (NEWs) [14]. Figure 5 illustrates

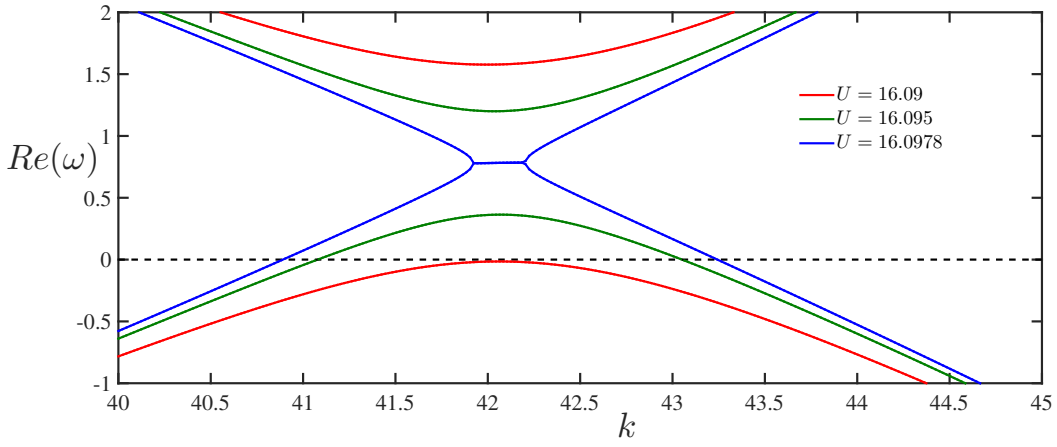

Figure 3. The magnified fragment of Fig. 2 for the same set of parameters.

Preprints (www.preprints.org) | NOT PEER-REVIEWED | Posted: 2 November 2021 doi:10.20944/preprints202111.0042.v1

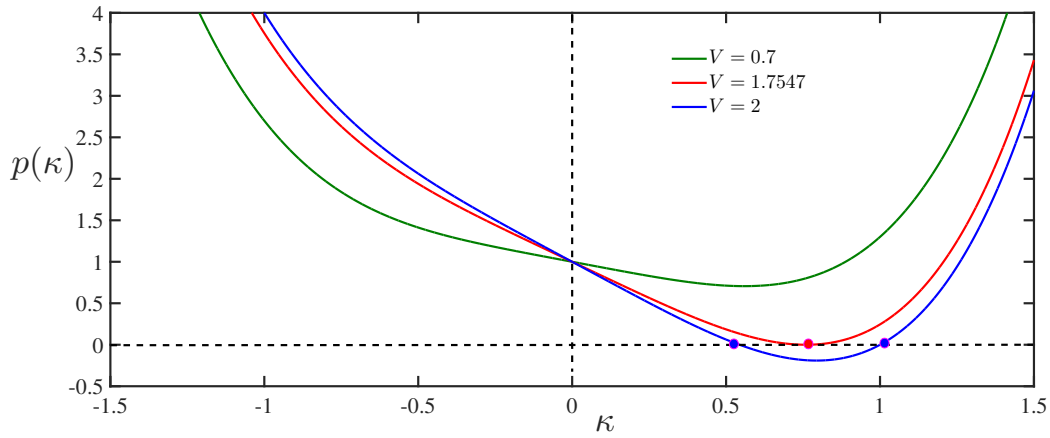

Figure 4. (Color online) The shape of the polynomial $p(\kappa)$ for three different values of V. Line 1, $V = 0.7$, – no real roots; line 2, $V = 1.7547$, – there is one double root (designated by red dot); line 3, $V = 2.0$, – there are two real roots (designated by blue dots).

the same dispersion curves as in Fig. 2 for $\omega \geq 0$ with k being of either sign. In this representation, the negative frequency ω is associated with the negative energy wave. However, the waves with the 'negative frequency' and negative wavenumber k are qualitatively similar and propagate in the same direction as for waves with positive frequency and positive wavenumber k.

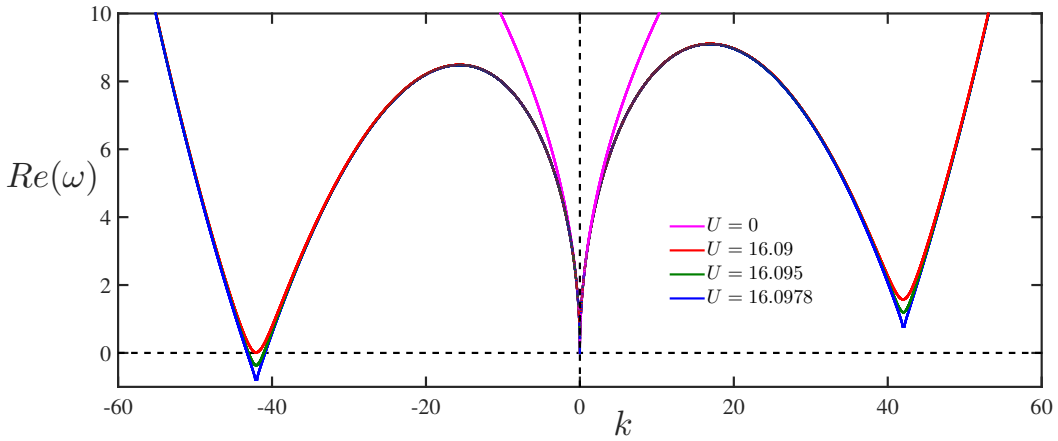

Figure 5. Non-symmetric branches of dispersion curves corresponding to waves propagating in the opposite direction. Note that the pink and blue lines have negative portions, which correspond to NEWs.

Figure 3 reveals that with an increase in the values of wind speed U beyond U_{c1}, the upper and lower branches of the dispersion curves continue to coverge to each other and ultimately reconnect at $U = U_{KH}$ where $U_{KH} = U_{c1}\sqrt{1+a}$. It may be noted that the density ratio in the case of air-water interface is chosen as $a = 0.0012$ to ensure $U_{KH} \approx 1.0006 U_{c1}$. Besides, the Kelvin–Helmholtz-type (KH) instability occurs when the

Preprints (www.preprints.org) | NOT PEER-REVIEWED | Posted: 2 November 2021 doi:10.20944/preprints202111.0042.v1

wind speed U exceeds U_{KH}. Moreover, the instability occurs in the interval $k_1 \leq k \leq k_2$, where k_1 and k_2 can be derived from the following fifth-degree polynomial equation

$$\frac{r\,d\,D}{\rho_2}k^5 + (1+a)\frac{D}{\rho_2}k^4 - a\,r\,d\,U^2k^2 + \Big[(1-a)r\,d\,g - aU^2\Big]k + (1-a^2)\,g = 0. \tag{14}$$

This type of reconnection is significant for the interaction of waves with opposite energy signs which leads to the occurrence of K–H instability [14,15]. This phenomenon is attributed to the exchange of wave energy between the positive and negative energy waves associated with the upper and lower branches of the dispersion relation respectively. Consequently, the amplitudes of both the waves synchronously grow in time.

Besides, in the interval $U_{c1} < U < U_{KH}$, no K–H instability occurs, whilst there exist non-growing but potentially unstable NEWs (see Fig. 3). Further, it may be noted that the wave amplitudes will grow for wavenumber k lying in the range $k_1' < k < k_2'$ provided their associated energy decreases. Moreover, from Eq. (13) it is clear that the velocities U_{c1} and U_{KH} are closed to each other for smaller values of density ratio a, which happens in the case of air-water interface for $a = 0.0012$. It is pertinent to mention that Benjamin [20] was the first who discovered that for $a \simeq 1$, $U_{c1} \simeq U_{KH}/\sqrt{2}$, which is typical for internal layers in the oceans or the atmosphere.

Although the parameters for rubber ice are not well defined, it is of interest to demonstrate the influence of this parameter on the dispersion properties of NEWs. In the context of the present study, the value of Young modulus is chosen as $E = 10^7$ Pa, which is close to India rubber. Figure 6 illustrates the dispersion curves of NEWs for three different values of Young modulus with airflow velocity $U = 16.09$ m/s. Figure 6 reveals that the dispersion curve has no optima for $E = 10^6$ Pa, whereas the lower branch of the dispersion curve attains zero minima for $E = 10^7$ Pa and KH instability occurs for $E = 10^8$ Pa. Thus, it is concluded that the critical wind speed varies with the change in the values of Young's modulus E which is also clear from Eq. (13).

NEWs are neutrally stable in the absence of energy dissipation. However, they can grow in time only if there is a mechanism for taking out their energy. Potentially, there are different mechanisms responsible for the growth of NEWs. In particular, similar to the dissipative instability in plasma [21], viscous dissipation in the immovable lower layer leads to the growth of NEWs [22]. The dissipation of wave energy leading to the growth of NEWs and shear flow instability can be related to the radiation of internal waves from the pycnocline in the density stratified ocean [23]. For amplification of NEWs, viscosity must lead to "positive losses". For example, the NEWs in the model considered is damped if the upper moving layer is viscous rather than the lower layer. On the other hand, as the viscosity in the moving upper layer leads to "negative damping", the positive energy waves can grow on the upper branch of the dispersion curve. Undoubtedly, when the upper layer is at rest

Preprints (www.preprints.org) | NOT PEER-REVIEWED | Posted: 2 November 2021 doi:10.20944/preprints202111.0042.v1

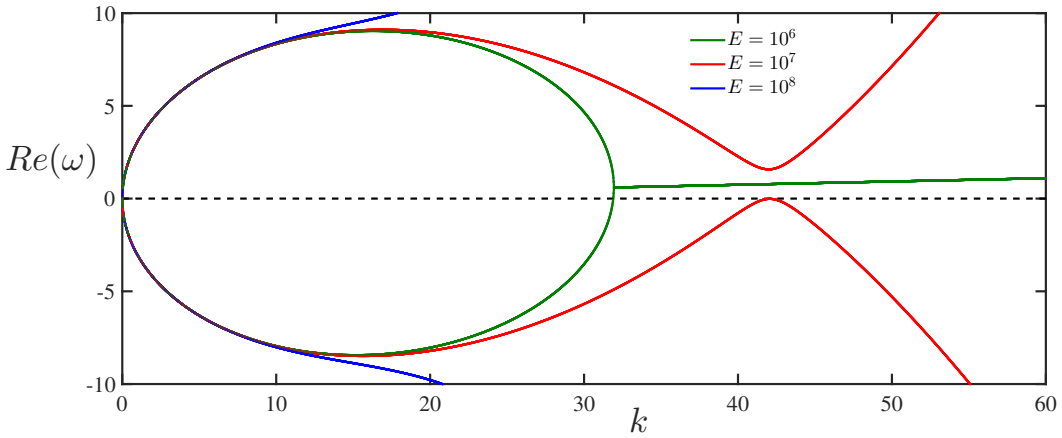

Figure 6. Influence of ice elasticity on the dispersion curves for the particular airflow velocity $U = 16.09$ m/s.

in the reference system, the energy associated with the growth as well as dissipative modes change signs simultaneously [14]. In such a reference system, NEWs exist on the upper branch of the dispersion curve, which can grow under the influence of positive dissipation. Besides, the shear flow instability associated with this mode remains unchanged to the choice of the reference system.

It is interesting to note that by using simple transformation $\omega \to \omega + kU$ in Eq. (9), the dispersion relation associated with the stationary upper layer and oppositely moving lower layer can be obtained as

$$G_2(\omega, k) \equiv \frac{\rho_1}{k}\omega^2 + \frac{\rho_2}{k}(1 + r\,d\,k)(\omega + kU)^2 + (\rho_1 - \rho_2)g - Dk^4 = 0. \tag{15}$$

Proceeding in a similar manner as in the case of Eq. (13), it can be easily concluded that NEWs arise for a very small velocity of the moving lower layer with current speed $U > U_{c2}$ where

$$U_{c2} = \left[\frac{4}{3}\frac{1-a}{a}g\left(\frac{4D}{\rho_2}\right)^{1/3}\right]^{3/8}. \tag{16}$$

It is noteworthy to mention that the critical velocities U_{c1} and U_{c2} as in Eqs. (13) and (16) are very close to each other in the case of $a \simeq 1$ (e.g., for internal waves on the ocean pycnocline). However, it is significant for $a \ll 1$ where U_{c1} is much greater than U_{c2} with $U_{c2} \approx 0.545$ m/s and $U_{c1} \approx 16.09$ m/s as considered in the present study. A fragment of the dispersion curve associated with Eq. (15) in the frame co-moving with the upper layer (i.e., static upper layer and moving lower layer) is exhibited in Fig. 7 for different values of U including $U_{c2} = 0.545$ m/s. In general, Fig. 7 reveals that the NEWs can exist on both branches of the dispersion curves for waves that are slowed down relative to the flow with phase velocities being lower than the velocities of the associated fluid layer.

Preprints (www.preprints.org) | NOT PEER-REVIEWED | Posted: 2 November 2021 doi:10.20944/preprints202111.0042.v1

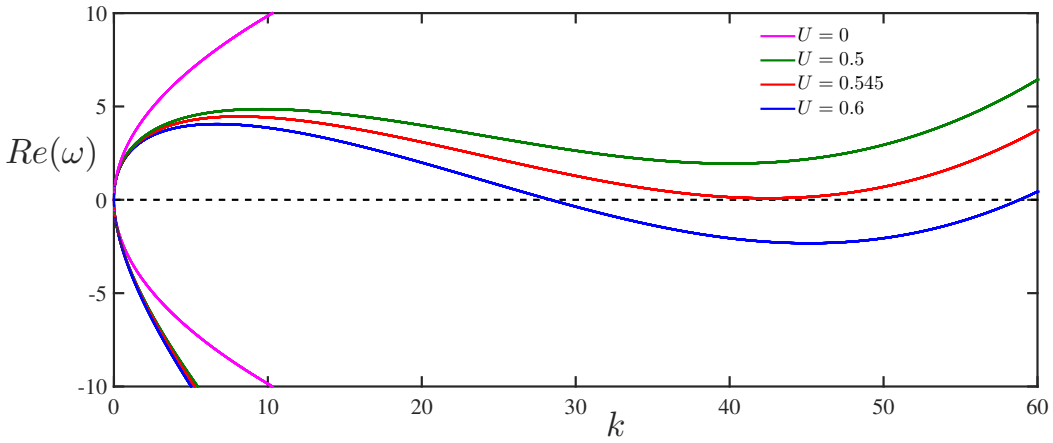

Figure 7. Dispersion relation (15) in the frame co-moving with the upper layer (air) for a few values of U.

3. Modulation instability of hydro-elastic waves at the interface on the tangential discontinuity of a shear flow

In the present section, our emphasis is to derive the general structure of the nonlinear equation in terms of the interfacial perturbation at the air-water interface which is covered by rubber ice followed by a derivation of the nonlinear Schrödinger equation. In addition, the criteria for the modulation instability will be determined and analysed.

3.1. General solution of velocity potentials

In this section, the perturbation of the air-water interface is assumed to be small in the form of Eq. (7), whereas the amplitude A is considered to be a slowly varying function of space x and time t. Proceeding in a similar manner as in Eq. (8), we look for the solutions of the velocity potentials, including the nonlinear dependencies of the functions $\Phi_j(z)$ for $j = 1, 2$ on the perturbation of the interface η, following the approach adopted in [8,24]. Using the kinematic boundary conditions as in Eqs. (4), (5) and (6) along with the vertical boundary condition for $|z| \to \infty$ as in Eqs. (2) and (3), the velocity potentials are derived in the form

$$\Phi_1(x,z,t) = -\frac{\eta_t + U\eta_x}{k(1+\mathrm{i}\eta_x)}e^{-kz} = -\frac{e^{-kz}}{k}(\eta_t + U\eta_x)\Big(1 - \mathrm{i}\eta_x - \eta_x^2 + \ldots\Big), \tag{17}$$

$$\Phi_2(x,z,t) = \frac{\eta_t}{k(1-\mathrm{i}\eta_x)}e^{kz} = \frac{e^{-kz}}{k}\eta_t\Big(1 + \mathrm{i}\eta_x - \eta_x^2 + \ldots\Big). \tag{18}$$

Substituting the solutions for Φ_1 and Φ_2 as in Eqs. (17) and (18) into the dynamic boundary condition as given in Eq. (6), the following nonlinear equation in terms of η (up to third order) is obtained as

$$G_1(\omega,k)\eta = \alpha(\omega,k)\eta^2 + \beta(\omega,k)\eta^3, \tag{19}$$

Preprints (www.preprints.org) | NOT PEER-REVIEWED | Posted: 2 November 2021 doi:10.20944/preprints202111.0042.v1

where

$$\alpha(\omega,k) = \rho_2(1+r\,d\,k)\omega^2 - \rho_1(\omega - kU)^2, \tag{20}$$

$$\beta(\omega,k) = -k\Big[\rho_1(\omega - kU)^2 + \rho_2(1+r\,d\,k)\omega^2\Big]. \tag{21}$$

and $G_1(\omega,k)$ is given in Eq. (9). By neglecting the higher order terms of η in Eq. (19), the dispersion relation is obtained as $G_1(\omega,k) = 0$. Using the dispersion relation as in Eq. (10), the coefficients of the nonlinear terms α and β in Eqs. (20) and (21) for the lower ($j = 1$) and upper ($j = 2$) branches of the dispersion curves are obtained as

$$\alpha_1(k) = \rho_2 \frac{\Big(\sqrt{\mathscr{D}} + akU\Big)^2(1+r\,d\,k) - a\Big(\sqrt{\mathscr{D}} - kU(1+r\,d\,k)\Big)^2}{(1+a+r\,d\,k)^2}, \tag{22}$$

$$\alpha_2(k) = \rho_2 \frac{\Big(\sqrt{\mathscr{D}} - akU\Big)^2(1+r\,d\,k) - a\Big(\sqrt{\mathscr{D}} + kU(1+r\,d\,k)\Big)^2}{(1+a+r\,d\,k)^2}, \tag{23}$$

$$\mathscr{D}(k) = (1+a+r\,d\,k)\Big[(1-a)gk + Dk^5/\rho_2\Big] - ak^2U^2(1+r\,d\,k), \tag{24}$$

$$\beta_1(k) = \beta_2(k) = -k^2[Dk^4 + (1-a)g\rho_2]. \tag{25}$$

The nonlinear terms in Eq. (19) provides the second harmonic as well as the mean flow generation by the quasi-sinusoidal primary-harmonic wave.

3.2. Derivation of the NLS equation for the HEWs

Unlike the velocity potentials are expanded in terms of the perturbational amplitude which has been assumed to be a slowly varying function of space and time, method of multiple scales are being used here to obtain the nonlinear Schrödinger (NLS) equation by introducing 'fast' and 'slow' variables along with a non-dimensional small parameter ε with $\varepsilon \ll 1$ such that

$$t_n = \varepsilon^n t, \quad x_n = \varepsilon^n x, \quad n = 0,1,2. \tag{26}$$

Here, t_0, x_0 represent fast variables, and t_1, x_1, t_2, and x_2 are slow ones. Consequently, the differential operators $\partial/\partial t$ and $\partial/\partial x$ are expressed via derivative expansions in the following forms

$$\frac{\partial}{\partial t} = -\omega\frac{\partial}{\partial\theta_0} + \varepsilon\frac{\partial}{\partial t_1} + \varepsilon^2\frac{\partial}{\partial t_2} + \ldots, \tag{27}$$

$$\frac{\partial}{\partial x} = k\frac{\partial}{\partial\theta_0} + \varepsilon\frac{\partial}{\partial x_1} + \varepsilon^2\frac{\partial}{\partial x_2} + \ldots, \tag{28}$$

Preprints (www.preprints.org) | NOT PEER-REVIEWED | Posted: 2 November 2021 doi:10.20944/preprints202111.0042.v1

where $\theta_0 = kx_0 - \omega t_0$ with ω and k being related with the dispersion relation (10). Using the expansion as in Eqs. (27) and (28), the linear part of Eq. (19) is represented through the operator of the form

$$\hat{L}\left[(-\mathrm{i}\omega, \mathrm{i}k) + \varepsilon\left(\frac{\partial}{\partial t_1}, \frac{\partial}{\partial x_1}\right) + \varepsilon^2\left(\frac{\partial}{\partial t_2}, \frac{\partial}{\partial x_2}\right) + \ldots\right],$$

which can be expanded in terms of ε and its powers about the point $(-\mathrm{i}\omega, \mathrm{i}k)$ as

$$\hat{L} = \hat{L}_0 + \varepsilon\hat{L}_1 + \varepsilon^2\hat{L}_2 + \ldots.$$

Thus, under the assumption of the linear approximation from Eq. (19) it can be easily derived that

$$\hat{L}\eta = \left(\hat{L}_0 + \varepsilon\hat{L}_1 + \varepsilon^2\hat{L}_2 + \ldots\right)\eta = 0. \tag{29}$$

Further, the perturbation of the air-water interface η can be expanded in the form of following series as

$$\eta(x,t) = \sum_{n=1}^{3} \varepsilon^n \eta_n(\theta_0, x_1, x_2; t_1, t_2) + O(\varepsilon^4). \tag{30}$$

Substituting Eqs. (29) and (30) in Eq. (19), the linear and successive higher orders of partial differential equations can be obtained by equating the components of equal powers of ε:

$$\begin{aligned}
O(\varepsilon) &: L_0\eta_1 = 0;\\
O(\varepsilon^2) &: L_0\eta_2 = -L_1\eta_1 + \alpha\eta_1^2;\\
O(\varepsilon^3) &: L_0\eta_3 = -L_1\eta_2 - L_2\eta_1 + 2\alpha\eta_1\eta_2 + \beta\eta_1^3.
\end{aligned}$$

Under the assumption of lowest-order approximation, a quasi-monochromatic perturbation solution is considered in the case of slowly varying amplitude and is given by (cf. Eq. (7))

$$\eta_1 = A(x_1, x_2; t_1, t_2)e^{\mathrm{i}\theta_0} + c.c.$$

Proceeding in a similar manner η_2 is obtained as

$$L_0\eta_2 = -\mathrm{i}\left(\frac{\partial G_1}{\partial\omega}\frac{\partial A}{\partial t_1} - \frac{\partial G_1}{\partial k}\frac{\partial A}{\partial x_1}\right)e^{\mathrm{i}\theta_0} + \alpha A^2 e^{2\mathrm{i}\theta_0} + c.c.$$

The coefficient of $e^{i\theta_0}$ represents a secular term in this equation. This secular term eliminated by using the solvability criteria

$$\frac{\partial G_1}{\partial\omega}\frac{\partial A}{\partial t_1} - \frac{\partial G_1}{\partial k}\frac{\partial A}{\partial x_1} = 0.$$

Preprints (www.preprints.org) | NOT PEER-REVIEWED | Posted: 2 November 2021 doi:10.20944/preprints202111.0042.v1

Using the definition of group velocity $c_g = \frac{d\omega}{dk} = -\frac{\partial G_1}{\partial k} / \frac{\partial G_1}{\partial \omega}$, the solvability criteria is rewritten as

$$\frac{\partial A}{\partial t_1} + c_g \frac{\partial A}{\partial x_1} = 0. \tag{31}$$

Using this condition, a uniformly valid expansion of η_2 can be written in the form

$$\eta_2 = \frac{\alpha A^2}{G_1(2\omega, 2k)} e^{2i\theta_0} + c.c.$$

Using the expression of $G_1(\omega, k)$ as in Eq. (9), the function $G_1(2\omega, 2k)$ corresponding to both the upper and lower branches of dispersion curves is obtained as

$$G_1(2\omega(k), 2k) = \rho_2 \Bigg\{ \frac{2a}{k} \left(kU - \frac{\sqrt{\mathscr{D}} + akU}{1 + a + r\,d\,k} \right)^2 - \frac{16D}{\rho_2} k^4 - (1-a)g + \frac{2}{k} \frac{(1 + 2r\,d\,k)(\sqrt{\mathscr{D}} + a\,k\,U)^2}{(1 + a + r\,d\,k)^2} \Bigg\}.$$

Proceeding in a similar manner, from the third-order approximation of the parameter ε i.e., $O(\varepsilon^3)$, the solvability criteria for $L_0\eta_3$ is derived as

$$\mathrm{i}\left(\frac{\partial G_1}{\partial \omega} \frac{\partial A}{\partial t_2} - \frac{\partial G_1}{\partial k} \frac{\partial A}{\partial x_2} \right) = \frac{1}{2} \frac{\partial^2 G_1}{\partial \omega^2} \frac{\partial^2 A}{\partial t_1^2} - \frac{\partial^2 G_1}{\partial \omega \partial k} \frac{\partial^2 A}{\partial x_1 \partial t_1} + \frac{1}{2} \frac{\partial^2 G_1}{\partial k^2} \frac{\partial^2 A}{\partial x_1^2} + \left(\frac{2\alpha^2}{G_1(2\omega, 2k)} + \beta \right) |A|^2 A. \tag{32}$$

Further, the solvability criterion in Eq. (31) can be rewritten as

$$\frac{\partial^2 A}{\partial t_1^2} = c_g^2 \frac{\partial^2 A}{\partial x_1^2}. \tag{33}$$

Setting $x_n = \varepsilon^n x$ and $t_n = \varepsilon^n t$, and using Eq. (33) in Eq. (32), the NLS is obtained as

$$\mathrm{i}\left(\frac{\partial A}{\partial t} + c_g \frac{\partial A}{\partial x} \right) + P \frac{\partial^2 A}{\partial x^2} + \varepsilon^2 Q |A|^2 A = 0, \tag{34}$$

where the dispersion coefficient P and nonlinear coefficient Q are given by [7,25]

$$P = \frac{1}{2} \frac{dc_g}{dk}, \qquad Q = -\left(\frac{2\alpha^2}{G_1(2\omega, 2k)} + \beta \right) \left(\frac{\partial G_1}{\partial \omega} \right)^{-1}.$$

Next, substituting the new variable $b = \varepsilon A$, the final form of the NLS equation is obtained as

$$\mathrm{i}\left(\frac{\partial b}{\partial t} + c_g \frac{\partial b}{\partial x} \right) + P \frac{\partial^2 b}{\partial x^2} + Q |b|^2 b = 0. \tag{35}$$

Preprints (www.preprints.org) | NOT PEER-REVIEWED | Posted: 2 November 2021 doi:10.20944/preprints202111.0042.v1

4. Modulation instability of HEWs

In this section, the expressions for the dispersion coefficient P and nonlinear coefficients Q, as defined in Eq. (35), will be derived in two different cases for the lower and upper branches of the dispersion curves associated with Eq. (10), for determining the criteria of modulation instability.

4.1. NLS equation and modulation instability in the lower branch of the dispersion curve

In the present subsection, the frequency ω_2 corresponding to the lower branch of the dispersion curve is used to derive the expressions of the dispersion coefficient P_l and the nonlinear coefficient Q_l in the NLS Eq. (35), and are given by

$$P_l = \frac{A^2}{8B^{3/2}(1+a+R)} - \frac{r^2d^2(\sqrt{B}-a\,k\,U)}{(1+a+R)^3} - \frac{r\,d\left(a\,U+\dfrac{A}{2\sqrt{B}}\right)}{(1+a+R)^2} + \frac{2aU^2(1+R)+2r\,d\,C-20(1+a+R)Dk^3/\rho_2+4a\,r\,d\,k\,U^2}{4\sqrt{B}(1+a+R)}, \tag{36}$$

$$Q_l = -\frac{k^2}{2\sqrt{k(Dk^4+g\rho_2-ag\rho_2)B_1-C_1\rho_2^2}} \times\left\{F_1k+\frac{2\rho_2\left[a\left(kU+\rho_2\dfrac{A_1}{B_1}\right)^2-\rho_2R_1\dfrac{A_1^2}{B_1^2}\right]^2}{(1-a)gk+16k^5\dfrac{D}{\rho_2}-2a\left(kU+\rho_2\dfrac{A_1}{B_1}\right)^2-2\rho_2^2(1+2d\,k\,r)\dfrac{A_1^2}{B_1^2}}\right\}, \tag{37}$$

where $A=(1+a+R)C-rdF+2aU^2(1+F)k+ardk^2U^2$, $B=(1+a+R)F-ak^2U^2(1+R)$, $C=g(a-1)-5Dk^4/\rho_2$ $F=Dk^5/\rho_2+(1-a)gk$, $R=rdk$, $A_1=\sqrt{kB_1F_1/\rho_2^2-C_1}-akU$, $B_1=(1+a)\rho_2+\rho dk$, $C_1=ak^2U^2R_1/\rho_2$, $F_1=Dk^4+(1-a)\rho_2g$, $R_1=\rho_2+\rho dk$.

In particular, for $a=U=D=\rho_i=0$, the dispersion relation (10), corresponding group velocity, dispersion and nonlinear coefficients P_l and Q_l reduce to

$$\omega_2=-\sqrt{gk},\quad c_g=-\frac{1}{2}\sqrt{\frac{g}{k}},\quad P_l=\frac{1}{8}\sqrt{\frac{g}{k^3}},\quad Q_l=\frac{1}{2}\sqrt{gk^5}, \tag{38}$$

where the coefficients P_l and Q_l are analogous to the coefficients of the NLS equation for surface gravity waves in deep water [26–28].

It is interesting to that the dispersion and nonlinear coefficients of NLS equation corresponding to the deep water flexural gravity wave covered by an ice plate can be easily derived from Eqs. (36) and (37) by putting $a=0$ and $U=0$, which was studied recently by [12].

In Figs. 8 and 9, the dependencies of $P_l(k)$ and $Q_l(k)$ are demonstrated in the lower branch of the dispersion curve for different values of wind speed with $U=0$, $U=U_{c1}=16.09$

Preprints (www.preprints.org) | NOT PEER-REVIEWED | Posted: 2 November 2021 doi:10.20944/preprints202111.0042.v1

m/s, and $U = U_{KH} \approx 16.10$ m/s. Figure 8 reveals that the dispersion coefficient $P_l(k)$ has only one root for all values of U where its sign changes from positive to negative. On the other hand, Fig. 9 depicts that the nonlinear coefficient $Q_l(k)$ has a singularity at $k = k_s \approx 29.1$ 1/m for all values of U, where $Q_l(k)$ changes its sign from positive to negative. It is worth mentioning that both the functions $P_l(k)$ and $Q_l(k)$ attain their minima around the point $k \approx 42$ 1/m where K–H instability occurs for $U = U_{KH}$. The minima become deeper and deeper when U approaches U_{KH}, and in the limit, $U \to U_{KH}$, the singularities appear in both the functions $P_l(k)$ and $Q_l(k)$.

As per Lighthill criterion, a uniform wavetrain becomes unstable with respect to self-modulation in the case of the function $W_l(k) \equiv P_l(k)Q_l(k)$ is positive [29,30]. Figure 10 demonstrates the zones of modulation stability (S) and instability (US) in the (k, U) plane. Furthermore, a dramatic change in this stability diagram is observed for the wind speed U higher than the critical value $U_m = 8.19$ m/s, which is because of the fact that the nonlinear coefficient $Q_l(k)$ has several roots. This results in the multiple changes of sign in the product of the dispersive coefficient $P_l(k)$ and nonlinear coefficient $Q_l(k)$. Moreover, Fig. 10 corresponds to the modulation instability of deepwater flexural gravity waves for $U = 0$ and $a = 0$, which was studied recently by [12].

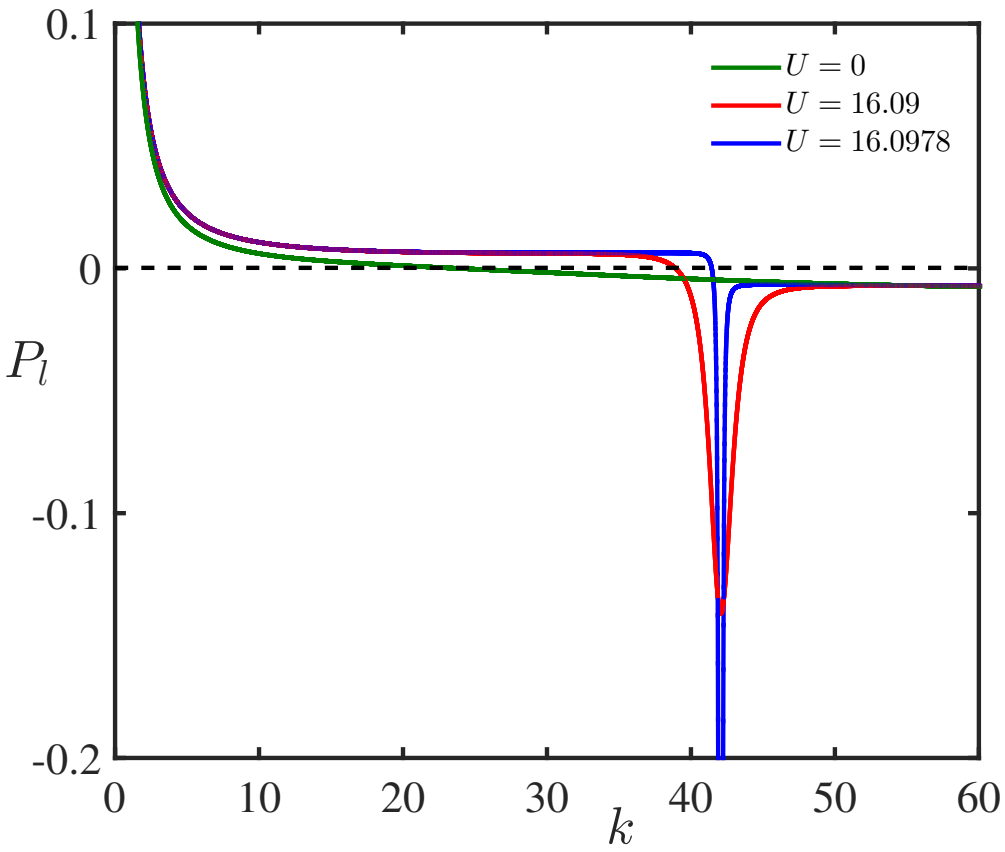

Figure 8. (Color online) Variation of dispersion coefficient $P_l(k)$ versus wavenumber k for different values of wind speed in the case of the lower branch of the dispersion curve

Preprints (www.preprints.org) | NOT PEER-REVIEWED | Posted: 2 November 2021 doi:10.20944/preprints202111.0042.v1

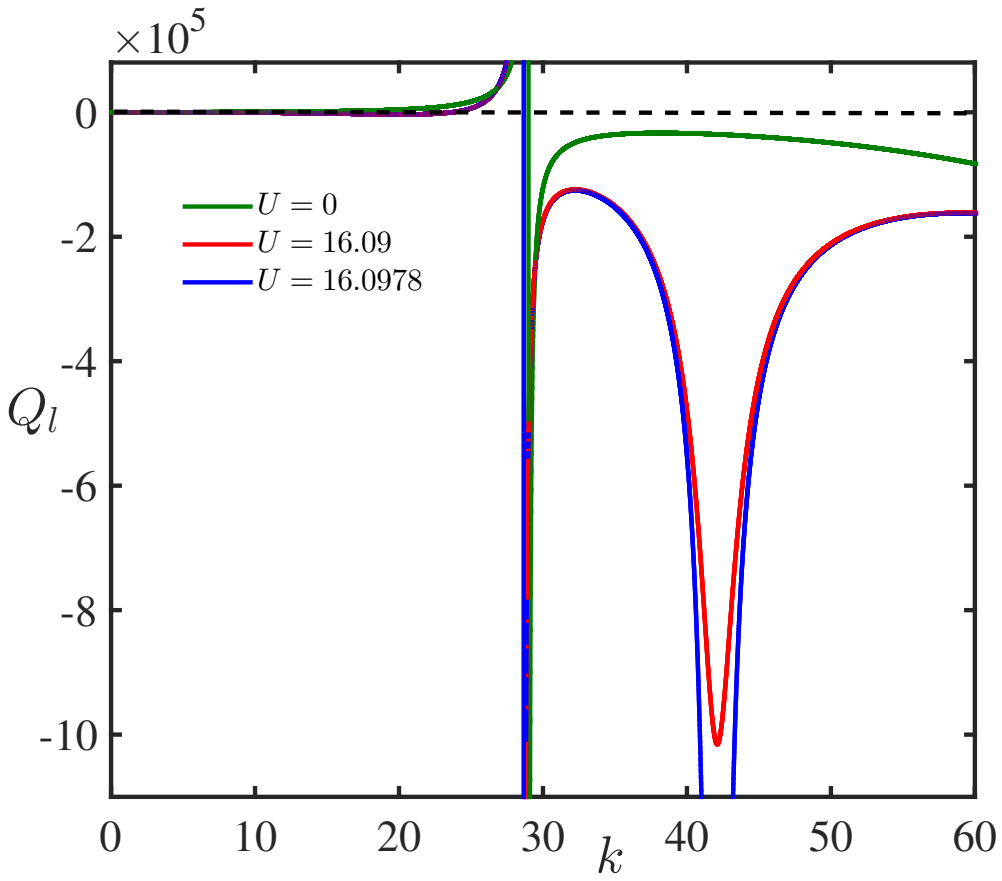

Figure 9. (Color online) Variation of the nonlinear coefficient Q_l versus wavenumber k for different values of wind speed U in the case of lower branch of dispersion curve.

It is worth mentioning that the maximum growth rate of modulation instability occurs for wavenumber of modulation $K_{max} = b_0\sqrt{Q_l/P_l}$ in the NLS equation (35), where b_0 is referred as the sinusoidal wave amplitude (see, e.g., [25]). Further, it is important to note that $I_{max} = |Q_l(k)|b_0^2$ is the maximal value of growth rate. Again, for a given value of U, this expression can be further optimized with respect to the carrier wavenumber k [31].

During the occurrence of modulation instability, envelope solitary waves (solitons), breathers, freak waves can emerge from certain initial perturbations; in addition to the occurrence of fascinating phenomena related to their interactions whose details can be found in [7,26,32]. Besides, in the case of modulational stability, dark solitons can be developed on the background of a quasi-sinusoidal wave [7]. Figure 11 demonstrates the examples of (a) bright and (b) dark solitary envelope waves.

The NLS equation (35) becomes inapplicable when its coefficients $P(k)$ or $Q(k)$ vanish. This occurs at the boundaries between the stable and unstable domains, which is exhibited in Fig. 10. Thus, the generalised NLS equation should be derived by taking into account the higher-order terms as in [33,34]. However, this is not considered in the present study and will be studied separately.

Preprints (www.preprints.org) | NOT PEER-REVIEWED | Posted: 2 November 2021 doi:10.20944/preprints202111.0042.v1

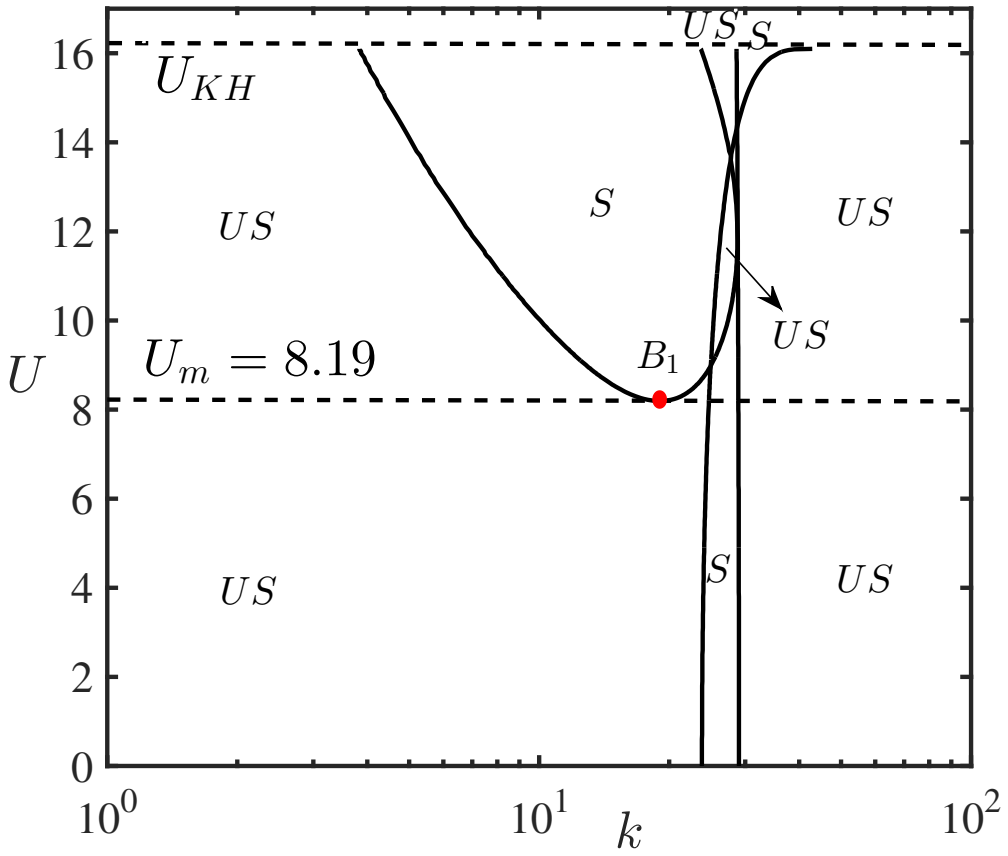

Figure 10. Zones of modulation stability (S) and instability (US) in the (k, U) plane. The dashed line on the top depicts the critical velocity $U_{KH} = 16.10$ 1/m at which the Kelvin–Helmholtz instability arises. The bifurcation point in the diagram is denoted by Q_1 for $U = U_m$.

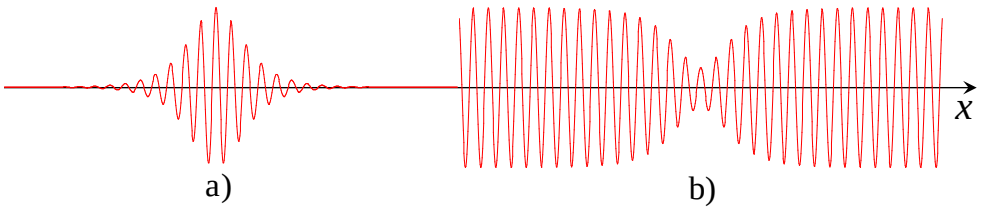

Figure 11. (Color online) Examples of (a) bright and (b) dark envelope solitons.

4.2. NLS equation and modulation instability in the upper branch of the dispersion curve

In the present section, the upper branch of the dispersion curve ω_1 as given in Eq. (10) is considered for the derivation of the dispersion and nonlinear coefficients P_u and Q_u and to determine the condition of modulation instability. As in the case of the lower branch of the

Preprints (www.preprints.org) | NOT PEER-REVIEWED | Posted: 2 November 2021 doi:10.20944/preprints202111.0042.v1

dispersion curve, the dispersive coefficient P_u and the nonlinear coefficient Q_u in the NLS Eq. (35) are obtained as

$$P_u = \frac{-1}{(1+a+R)}\left[\frac{A^2}{4B^{3/2}} - \frac{r^2d^2(\sqrt{B}+a\,k\,U)}{(1+a+R)^2} + \frac{r\,d}{1+a+R}\left(a\,U - \frac{A}{2\sqrt{B}}\right) + \frac{2a\,U^2(1+R)+2r\,d\,C-20(1+a+R)Dk^3/\rho_2+4a\,r\,d\,k\,U^2}{2\sqrt{B}}\right], \tag{39}$$

$$Q_u = \frac{k^2}{2\sqrt{k(Dk^4+g\,\rho_2-a\,g\,\rho_2)B_1-C_1\rho_2^2}} \times \left\{F_1k + \frac{2\rho_2\left[a\left(Uk-\rho_2\frac{P_1}{B_1}\right)^2-\rho_2R_1\frac{P_1^2}{B_1^2}\right]^2}{(1-a)g\,k+16k^5\frac{D}{\rho_2}-2a\left(k\,U-\rho_2\frac{P_1}{B_1}\right)^2-2\rho_2^2(1+2d\,k\,r)\frac{P_1^2}{B_1^2}}\right\}, \tag{40}$$

where $A, B, C, R, B_1, C_1, F_1$ and R_1 are same as in Eqs. (36) and (37) with $P_1 = \sqrt{kB_1F_1/\rho_2^2 - C_1} + akU$. The coefficients P_u and Q_u are exhibited in Figs. 12 and 13. A comparison of Figs. 8-9 with that of Figs. 12-13 reveals that the trend of the dispersion and nonlinear coefficients for the upper branch of the dispersion curves are opposite to that of P_l and Q_l.

Equations (39) and (40) attribute that the modulational instability occurs for positive values of the function $W_u(k) \equiv P_u(k)Q_u(k)$ associated with the upper branch of the dispersion curve. Figure 14 demonstrates the zones in (k, U) plane where the function $W_u(k)$ is positive and that leads to the occurrence of modulation instability. Further, the graphic begins to alter dramatically for U exceeds a critical limit $U_m = 9.4719$ m/s, which is because of the fact that Q_u has multiple roots where it changes sign in the case of wind speed $U > U_m$.

It is evident from Figs. 10 and 14 that the domains of modulation stability and instability are bizarrely interspersed on the diagram when U exceeds the critical value U_m in each branch of the dispersion curve. The importance of highlighting such domains is in the understanding of the existence of bright and dark envelopes of solitary waves. The former can arise in the process of the development of modulation instability, whereas the latter can appear in the modulational stable regions on the parameter plane. Moreover, in the case of modulation instability, rogue waves with extremely high amplitudes can emerge from rather regular initial perturbations [32]. The most important conclusion which can be derived from this study is the existence of modulational unstable waves of negative energy for wind speed in the range $U_{c2} < U < U_m$. Such waves can grow in time if a dissipative mechanism extracting energy from these waves is taken into account, for example, a turbulent viscosity of air which can be fairly significant. However, this issue is beyond the scope of the present study.

Preprints (www.preprints.org) | NOT PEER-REVIEWED | Posted: 2 November 2021 doi:10.20944/preprints202111.0042.v1

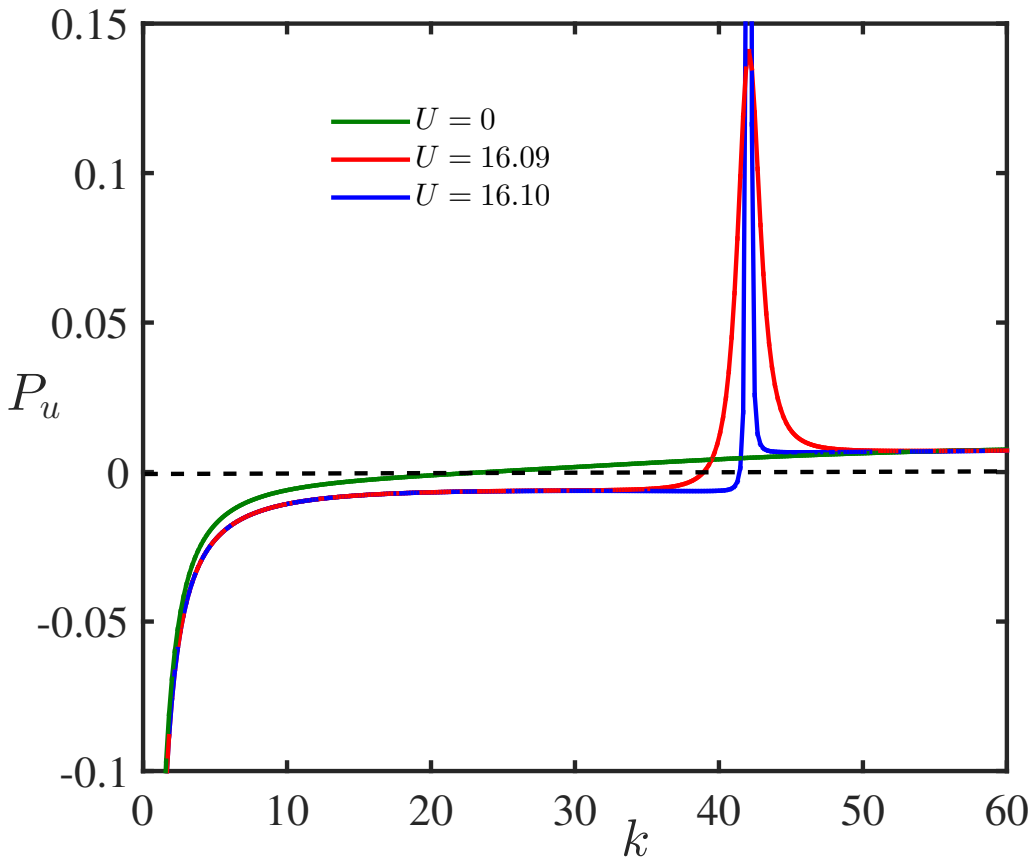

Figure 12. (Color online) Variation of the dispersion coefficient P_u versus wavenumber k for different values of wind speed in the case of upper branch of dispersion curve.

5. Conclusion

In the present manuscript, the criteria for modulation instability of hydro-elastic waves on the air-water interface are investigated under the influence of wind. The model considered is assumed to be the simplest model of wind with the uniform profile and tangential velocity discontinuity. However, this is a widely used canonical model of the flow in hydrodynamics, physical oceanography, geophysical fluid dynamics, plasma physics, and other fields. Despite the simplicity, the model provides an insight into the complicated range of phenomena occurring in the wave-current interactions. To the best of the authors' knowledge, the modulation instability of hydro-elastic waves under the influence of wind was not studied thus far. Thus, the present study has filled the said gap on modulation instability in the literature. The study exhibits the wavenumber range based on the current speed in which the stability and instability occur in the lower and upper branches of the dispersion curves. From the general model investigated here, limiting cases of pure gravity waves or flexural-gravity waves without airflow are reproduced. As a summary, an estimate of parameters of a modulated wave are presented with wavenumber $k = 10$ 1/ m ($\lambda = 2\pi/k \approx 0.63$ m), amplitude $\eta_0 = 0.01$ m and $U = 1$ m/s. Subsequently, the

Preprints (www.preprints.org) | NOT PEER-REVIEWED | Posted: 2 November 2021 doi:10.20944/preprints202111.0042.v1

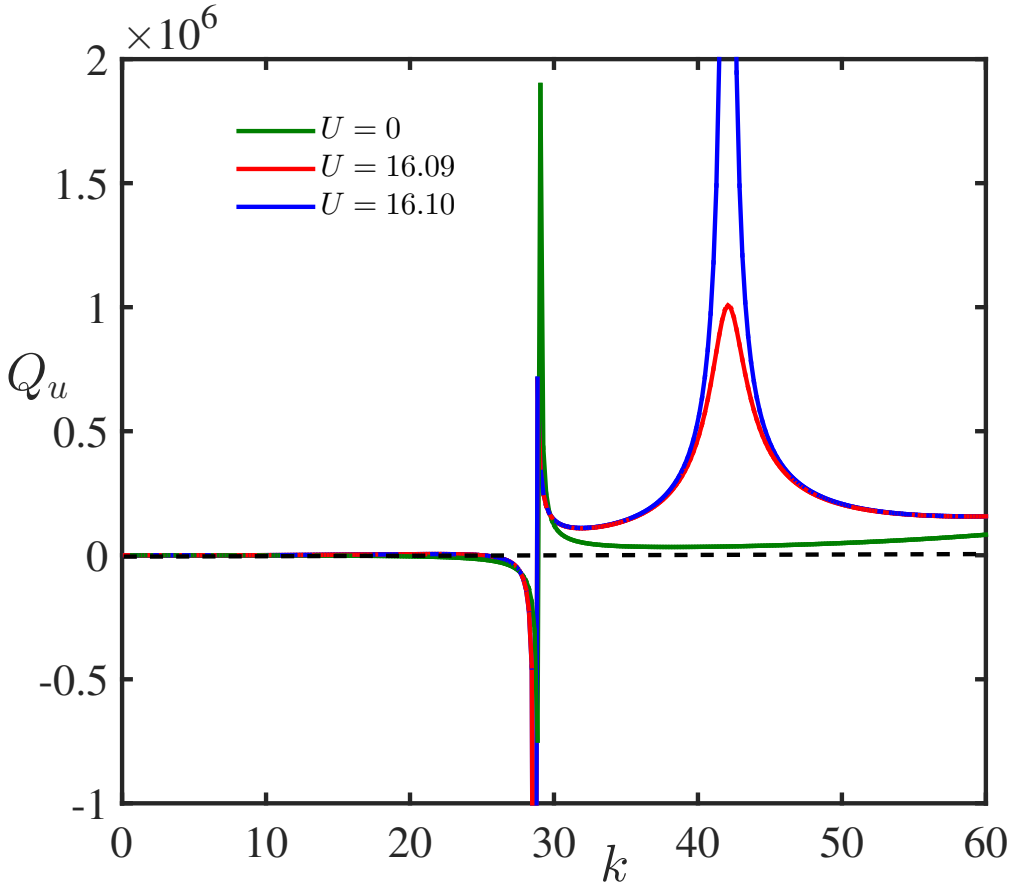

Figure 13. (Color online) Variation of the nonlinear coefficient Q_u versus wavenumber k for different values of wind speed in the case of upper branch of dispersion curve.

most rapidly increasing modulation wavenumber $K_{max} = \eta_0\sqrt{Q_u/P_u} \approx 2.01$ 1/m and wavelength $\Lambda = 2\pi/K_{max} \approx 3.12$ m are obtained. The maximal value of the growth rate is found to be $I_{max} = |Q(k)|\eta_0^2 \approx 0.05$ 1/s along with the characteristic time of wave growth $\tau = 1/I_{max} \approx 20.4$ s. These parameters look reasonable for the rubber ice and, they are practically insensible to the variation of the wind speed in the interval $U_{c2} < U < U_m$. The study can be generalized to deal with complex flow patterns including turbulent viscosity of air as well as the role of lateral compressive force on the floating ice sheet.

6. Acknowledgments

The authors gratefully appreciate partial funding from the Ministry of Human Resource and Development, Government of India, through the Apex Committee of SPARC, vide award number SPARC/2018-2019/P751/SL. S.B. gratefully acknowledges financial assistance from the Council of Scientific and Industrial Research, New Delhi, India, under the senior research fellowship vide file number. 09/081(1345)/2019-EMR-I. Y.S. appreciates the support of this work given by the Russian Federation's Ministry of Science and Higher Education's State Task Program in the Field of Scientific Activity (project No. FSWE-2020-

Preprints (www.preprints.org) | NOT PEER-REVIEWED | Posted: 2 November 2021 doi:10.20944/preprints202111.0042.v1

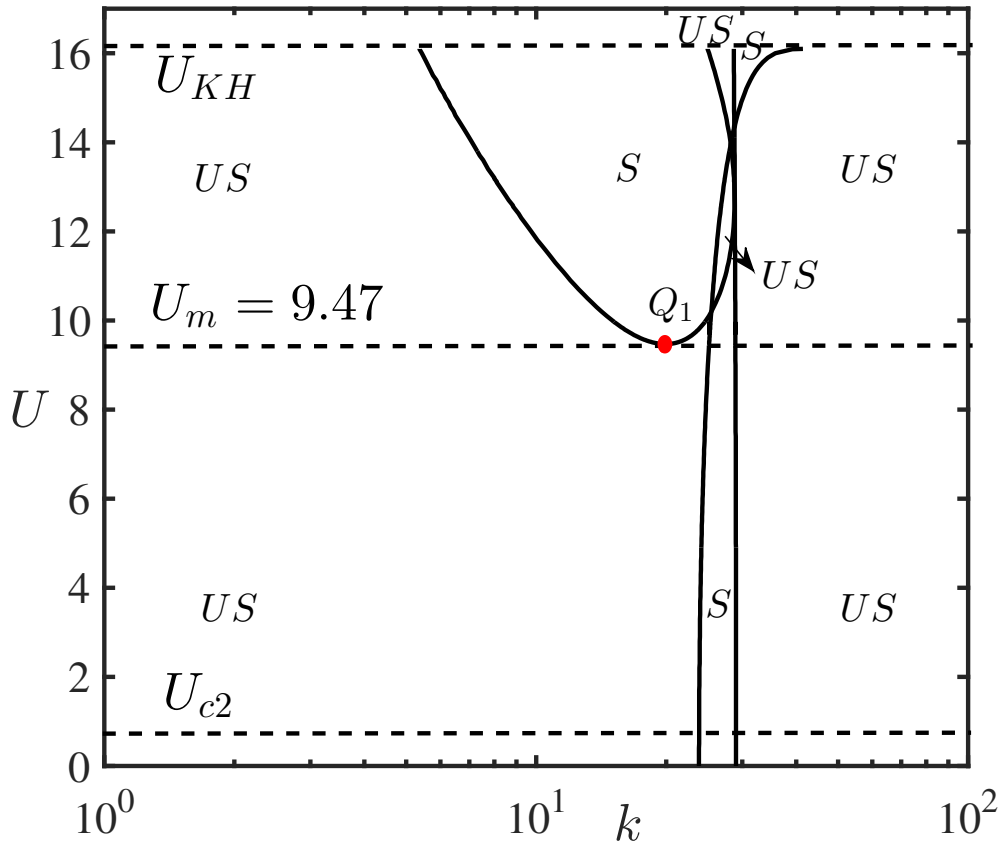

Figure 14. Modulation stability (S) and instability (US) zones in the (k, U) plane. The dashed line on the top depicts that the velocity corresponds to the K–H instability $U_{KH} = 16.0978$ m/s. The bifurcation point in the diagram is denoted by B_1 for $U = U_m$.

0007) and the grant of the President of the Russian Federation for the state support of Leading Scientific Schools of the Russian Federation (grant No. NSH-2485.2020.5).

References

1. Kheisin, D.Y. *Dynamics of Floating Ice Cover (in Russian. Technical English Translation in: FSTC-HT-23-485-69, U.S. Army Foreign Science and Technology Center)*; Gidrometeoizdat, Leningrad, 1967.
2. Squire, V.A.; Hosking, R.J.; Kerr, A.D.; Langhorne, P.J. *Moving Loads on Ice Plates*; Kluwer. Academ. Publ., Dordrecht, 1996.
3. Sahoo, T. *Mathematical Techniques for Wave Interaction with Flexible Structures*; CRC Press, Boca Raton, 2012.
4. Bukatov, A.E. *Waves in a Sea With a Floating Ice Cover (in Russian)*; FGBUN MHI, Sebastopol, 2017.
5. Djordjevic, V.D.; Redekopp, L.G. On two-dimensional packets of capillary-gravity waves. *J. Fluid Mech.* **1977**, *79*, 703–714.
6. Ablowitz, M.J.; Segur, H. On the evolution of packets of water waves. *J. Fluid Mech.* **1979**, *92*, 691–715.

7. Ablowitz, M.J.; Segur, H. *Solitons and the Inverse Scattering Transform*; SIAM: Philadelphia, USA, 1981.
8. Boral, S.; Sahoo, T.; Stepanyants, Y. Modulation instability of surface waves in the model with the uniform wind profile. *Symmetry* **2021**, *13*, 651.
9. Guyenne, P.; Părău, E.I. Finite-depth effects on solitary waves in a floating ice-sheet. *J. Fluids and Structures* **2014**, *49*, 242–262.
10. Il'ichev, A.T. Solitary wave packets beneath a compressed ice cover. *Fluid Dynamics* **2016**, *51*, 327–337.
11. Il'ichev, A.T. Effective wavelength of envelope waves on the water surface beneath an ice sheet: small amplitudes and moderate depths. *Theor. Math. Phys.* **2021**, *208*, 1182–1200.
12. Slunyaev, A.; Stepanyants, Y. Modulation property of flexural-gravity waves on a water surface covered by a compressed ice sheet. *ArXiv* **2021**.
13. Landau, L.D.; Lifshitz, E.M. *Fluid Mechanics*; Butterworth-Heinemann, Burlington, MA, 1987.
14. Fabrikant, A.L.; Stepanyants, Y.A. *Propagation of Waves in Shear Flows*; World Scientific Publishing Company, Singapore, 1998.
15. Ostrovski, L.A.; Rybak, S.A.; Tsimring, L.S. Negative energy waves in hydrodynamics. *Sov. Phys. Uspekhi* **1986**, *29*, 1040.
16. Ezersky, A.B.; Ostrovsky, L.A.; Stepanyants, Y.A. Wave-induced flows and their contribution to the energy of wave motions in a fluid. *Izv. Acad. Sci. USSR, Atmospheric and Oceanic Physics* **1981**, *17*, 890–895.
17. Miles, J.W. On the reflection of sound at an interface of relative motion. *J. Acoust. Soc. Amer.* **1957**, *29*, 226–228.
18. Ribner, H.S. Reflection, transmission and amplification of sound by a moving medium. *J. Acoust. Soc. Amer.* **1957**, *29*, 435–441.
19. Gelash, A.; Agafontsev, D.; Zakharov, V.; El, G.; Randoux, S.; Suret, P. Bound state soliton gas dynamics underlying the noise-induced modulational instability. *Phys. Rev. Lett.* **2019**, *123*, 890–895.
20. Benjamin, T.B. The threefold classification of unstable disturbances in flexible surfaces bounding inviscid flows". *J. Fluid Mech.* **1963**, *16*, 436–450.
21. Nezlin, M.V. Negative-energy waves and the anomalous Doppler effect. *Sov. Phys. Uspekhi* **1976**, *19*, 946.
22. Cairns, R.A. The role of negative energy waves in some instabilities of parallel flows. *J. Fluid Mech.* **1979**, *92*, 1–14.
23. Ostrovsky, L.A.; Stepanyants, Y.A.; Tsimring, L.S. Radiation instability in a stratified shear flow. *Int. J. Non-Lin. Mech.* **1983**, *19*, 151–161.
24. Abourabia, A.M.; Mahmoud, M.A.; Khedr, G.M. Solutions of nonlinear Schrödinger equation for interfacial waves propagating between two ideal fluids. *Can. J. Phys.* **2009**, *87*, 675–684.
25. Ostrovsky, L.A.; Potapov, A.I. *Modulated Waves: Theory and Applications*; The Johns Hopkins University Press,USA, 2002.
26. Yuen, H.C.; Lake, B.M. Nonlinear dynamics of deep-water gravity waves. *Adv. Appl. Mech.* **1982**, *22*, 67–229.

27. Peregrine, D.H. Water waves, nonlinear Schrödinger equations and their solutions. *ANZIAM J.* **1983**, *25*, 16–43.
28. Stiassnie, M. Note on the modified nonlinear Schrödinger equation for deep water waves. *Wave Motion* **1984**, *6*, 431–433.
29. Lighthill, M.J. Contributions to the theory of waves in nonlinear dispersive systems. *IMA J. Appl. Math.* **1965**, *1*, 269–306.
30. Lighthill, M.J. *Waves in Fluids*; Cambridge University Press, UK, 1978.
31. Grimshaw, R.; Stepanyants, Y. Emergence of envelope solitary waves from the initial localised pulses within the Ostrovsky equation. *Radiophys. Quantum Elect.* **2020**, *63*, 21–28.
32. Kharif, C.; Pelinovsky, E.; Slunyaev, A. *Rogue Waves in the Ocean*; Springer-Verlag Berlin Heidelberg, 2009.
33. Dysthe, K.B. Note on a modification to the nonlinear Schrödinger equation for application to deep water waves. *Proc. Roy. Soc. London A* **1979**, *369*, 105–114.
34. Trulsen, K.; Dysthe, K.B. A modified nonlinear Schrödinger equation for broader bandwidth gravity waves on deep water. *Wave Motion* **1996**, *24*, 281–289.